Estimating Moving Targets Behind Reinforced Walls Using Radar

Marija M. Nikolic, Arye Nehorai, *Fellow, IEEE*, and Antonije R. Djordjević

***Abstract*—We consider the estimation of moving targets located behind concrete walls reinforced with metallic bars, using radar measurements. The periodic structure of the rebar severely attenuates and distorts transmitted waveforms, which produces defocused images with ghost target estimates. We apply beamforming to estimate permittivity and thickness of the wall and number and position of the targets. The proposed solution is based on accurate physical models calculated using the method of moments. We show that the estimation is significantly improved by modeling the waveform distortion due to the bars. The resulting images are focused and clearly represent the contours of the targets. The algorithm is robust to the ambiguities in bar parameter values. In addition, the minimal necessary SNR is lower compared with the case in which the influence of the bars on the signal shape is ignored.**

***Index Terms*—Beamforming, periodic structure, reinforced wall, through-the-wall sensing.**

I. Introduction

An important task in urban warfare is using exterior electromagnetic sensing to detect people hidden inside buildings. Solving this problem is challenging because of the complex and unknown environment. The walls significantly attenuate and distort transmitted signals; hence electromagnetic modeling has an important influence on estimation accuracy. The distortion is particularly prominent in the case of walls reinforced by parallel steel bars (rods) or square-grid meshes, which are commonly used in construction [8]–[16]. We show that the complex, periodic structure of reinforced walls imposes significant difficulties in the target imaging that are not encountered in the case of homogenous walls. If the influence of the bars is not taken into account, images of the objects located behind the wall become defocused and false targets appear.

Several studies considered through-the-wall estimation [1]–[7]. In [1] and [2] the wall is treated as a homogeneous dielectric slab of known thickness and permittivity. The case in which the wall parameters are unknown is studied in [3]. The authors of [3] exploit measurements from two or more standoff distances from the wall to calculate images for various wall parameters. Assuming that the most focused image is obtained using accurate wall parameters, an image-focusing metric is applied to estimate the correct wall thickness and dielectric permittivity. Imaging through walls made of cinder block is addressed in [6]. The authors of this article consider the wall as a periodic structure and apply the SAR algorithm to estimate the target position. However, besides true target position, the SAR algorithm also produces a ghost target image. An estimation of the building layout is conducted in [7].

Electromagnetic propagation through reinforced concrete walls is well covered in the literature for the purpose of mobile channel modeling. Rigorous analysis of the transmission and reflection coefficients of reinforced walls has been carried out, e.g., in [8]–[10]. A non-destructive analysis of reinforced concrete using electromagnetic waves was conducted in [11]–[14]. Here, our focus is on estimating the position of the targets located behind reinforced walls. We separately investigate the cases of known and unknown wall parameters. We apply beamforming to the wideband measurements made by a sensor array to estimate wall thickness and dielectric permittivity. The number and positions of the targets are further estimated using beamforming [1], as well as wall-parameter estimates. In the case in which signal distortion due to the bars is not taken into account, the target spreads are large. We show that significant improvement is achieved when bar characteristics are partly or completely known. This improvement is particularly pronounced when the signal-to-noise ratio is low.

The organization of the paper is as follows. In Section II, we discuss the signal propagation through reinforced walls. We also present measurement models and our electromagnetic solver. Estimation of wall permittivity and thickness is discussed in Section III. In Section IV, we study moving-target estimation with unknown and known wall parameters. Finally, in Section V we present simulation results.

II. Signal Propagation Through Reinforced Walls

A. Reinforced Walls

Reinforced walls are generally one of two types: with bars or with mesh. When the incident electromagnetic field is parallel to the vertical bars, the horizontal bars (cross bars) have small influence on the transmission and reflection coefficient of the wall [8]. The same reasoning applies when the incident electric field is parallel to the horizontal bars. Therefore, without loss of generality, we consider a wall reinforced with vertical bars.

Manuscript received July 20, 2008; revised April 30, 2009. First published June 23, 2009; current version published November 04, 2009. This work was supported in part by the Department of Defense under Air Force Office of Scientific Research MURI Grant FA9550-05-1-0443, AFOSR Grant FA9550-05-1-0018, ONR Grant N000140810849, by COST Action IC0603 (Assist), and in part by Grant TR 11021 of the Serbian Ministry of Science and Technological Development.

M. M. Nikolic is with the Department of Electrical and Systems Engineering, Washington University in St. Louis, St. Louis, MO 63130 USA and also with the School of Electrical Engineering, University of Belgrade, Belgrade, Serbia (e-mail: nikolic2@ese.wustl.edu).

A. Nehorai is with the Department of Electrical and Systems Engineering, Washington University in St. Louis, St. Louis, MO 63130 USA (e-mail: nehorai@ese.wustl.edu).

A. R. Djordjević is with the School of Electrical Engineering, University of Belgrade, Serbia (e-mail: edjordja@etf.rs).

Digital Object Identifier 10.1109/TAP.2009.2025974

Report Documentation Page

Form Approved
OMB No. 0704-0188

1. REPORT DATE	2. REPORT TYPE	3. DATES COVERED
30 APR 2009		**00-00-2009 to 00-00-2009**

4. TITLE AND SUBTITLE	5a. CONTRACT NUMBER
Estimating Moving Targets Behind Reinforced Walls Using Radar	5b. GRANT NUMBER
	5c. PROGRAM ELEMENT NUMBER
6. AUTHOR(S)	5d. PROJECT NUMBER
	5e. TASK NUMBER
	5f. WORK UNIT NUMBER
7. PERFORMING ORGANIZATION NAME(S) AND ADDRESS(ES) **Washington University in St. Louis,Department of Electrical and Systems Engineering,St. Louis ,MO,63130**	8. PERFORMING ORGANIZATION REPORT NUMBER
9. SPONSORING/MONITORING AGENCY NAME(S) AND ADDRESS(ES)	10. SPONSOR/MONITOR'S ACRONYM(S)
	11. SPONSOR/MONITOR'S REPORT NUMBER(S)

12. DISTRIBUTION/AVAILABILITY STATEMENT
Approved for public release; distribution unlimited

13. SUPPLEMENTARY NOTES

14. ABSTRACT
see report

15. SUBJECT TERMS

16. SECURITY CLASSIFICATION OF:			17. LIMITATION OF ABSTRACT	18. NUMBER OF PAGES	19a. NAME OF RESPONSIBLE PERSON
a. REPORT **unclassified**	b. ABSTRACT **unclassified**	c. THIS PAGE **unclassified**	**Same as Report (SAR)**	**9**	

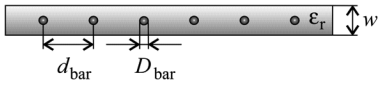

Fig. 1. Cross section of reinforced concrete wall.

We depict the cross section of such a wall in Fig. 1, where $d_{\rm bar}$ is the distance between adjacent bars (bar period), $D_{\rm bar}$ is the bar diameter, and w is the wall thickness. We assume the bars to be perfectly conducting and immersed in a homogeneous material (concrete) of relative dielectric permittivity $\varepsilon_{\rm r}$. We consider a two-dimensional problem, since electromagnetic modeling of electrically large structures, such as walls, is extremely time consuming.

B. Measurement Model

We determine the frequency response of the considered system using a surface formulation with the method of moments [17], [18]. The program that we developed uses the equivalence principle to divide the system under consideration into a number of subsystems (entities), each filled with a homogeneous medium. In our case, the system consists of sensors (line conductors whose cross section is electrically small) and dielectric walls with metallic bars inside. The program excites one sensor at a time by an impressed electric field, calculates the equivalent electric and magnetic currents on the surfaces of all entities, and evaluates the net electric currents in all probes. The results of the calculations are the impedance parameters (z) [19].

To model the measurements, we suppose a uniform linear array of M sensors placed in front of the reinforced wall. The array takes measurements at N known positions, at L frequencies. For 2D modeling, instead of induced voltages at the sensor ports we use the induced electric field in the sensors. The measured electric field in the ith sensor is

$$E_i(n,f_l)=\sum_{k=1}^{M}E_{ik}(n,f_l)+u,\quad i=1,\dots,M,\ n=1,\dots,N,\ l=1,\dots,L \quad (1)$$

where $E_{ik}(n,f_l)$ is the induced electric field in the ith sensor when the kth sensor is excited, f_l is the operating frequency, n is the index of the measurement position, and u is the measurement noise and modeling error. We assume complex, zero-mean Gaussian noise with variance σ^2.

The antenna array can be considered as a multiport network. If the impedance parameters are used, the measured induced electric field reads

$$E_i(n,f_l)=\sum_{k=1}^{M}z_{ik}(n,f_l)I_k(f_l)+u,\quad i=1,\dots,M,\ n=1,\dots,N,\ l=1,\dots,L \quad (2)$$

where $z_{ik}(k,f_l)$ is the mutual impedance coefficient between the ith and kth sensors, and I_k is the feeding current of the kth sensor. The feeding current is the same for all sensors. We assume Gaussian current excitation in the time domain. The magnitude of the pulse is 1A, and it is centered at $t=0$.

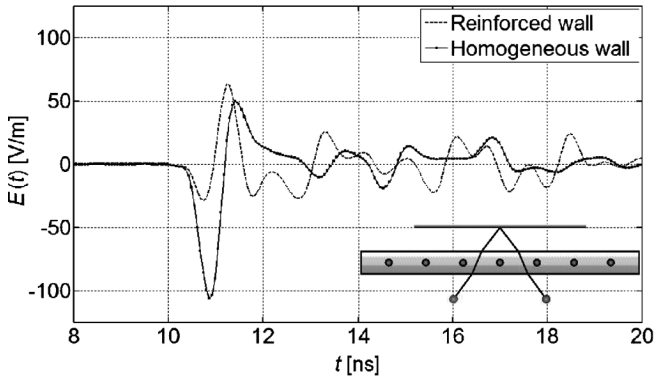

Fig. 2. Signals reflected from a perfectly conducting plane (PEC) located behind a reinforced wall and a homogeneous wall.

C. Time-Domain Response of Homogeneous and Reinforced Walls

The impulse response of concrete walls with rebar is investigated in [14], [20]. Until the signal reflected from the bars reaches the sensors, the reflected signals from a homogenous wall (without the rebar) and from the reinforced wall with the same dielectric permittivity are identical. Due to the multiple reflections from the bars, the signal reflected from the reinforced wall has an oscillating nature. These oscillations make the estimation of the objects behind the wall more difficult compared with the case of a homogeneous wall. The reinforcement does not introduce additional delay. We illustrate this property in Fig. 2, where we show the signals reflected from a perfectly conducting plane (PEC) placed behind a reinforced wall and behind a homogeneous wall. (The reflection from the PEC is obtained by subtracting the response of the wall from the response of the wall with the PEC behind.)

The simulated excitation waveform is a Gaussian pulse $g(t)=\mathrm{e}^{(-at)^2}$, where $a=3\mathrm{e}^{-9}\ \mathrm{s}^{-1}$. The pulse duration is 1.2 ns (pulse duration is defined as the time interval in which the signal amplitude is at least 5% of the maximum value). The frequency response is calculated from 5 MHz to 2 GHz in 5 MHz steps. (The usage of very low frequencies such as 5 MHz is not necessary for the through-the-wall imaging since the reflection coefficient of the reinforced wall is very high at those frequencies.)

We assume the wall thickness is $w=0.2$ m and the wall length is 8 m. The bar period is $d_{\rm bar}=0.15$ m and the bar diameter is $D_{\rm bar}=1$ cm. The permittivity of wall material is $\varepsilon_{\rm r}=3-\mathrm{j}0.15$. The transmitting-receiving pair is at a distance of 0.75 m from the front side of the wall, the separation between the sensors is 0.2 m, and the distance between the PEC and the sensors is 1.5 m.

III. Estimation of the Wall Dielectric Permittivity and Thickness Using Beamforming

A. Wall-Permittivity Estimation

Electromagnetic waves are reflected from interfaces of media with different electromagnetic properties. These reflections can be separated in the time domain if the sensors transmit sufficiently short pulses. The dielectric permittivity of the reinforced

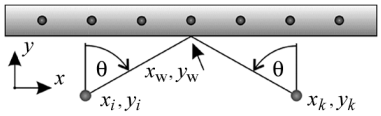

Fig. 3. Scheme used for wall-permittivity estimation.

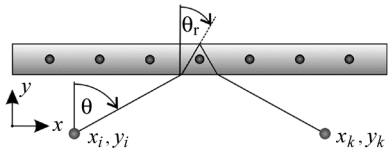

Fig. 4. Scheme used for wall-thickness estimation.

wall can be calculated in the same manner as the permittivity of the homogeneous wall in the time gate that ends when the signal reflected from the bars reaches the sensors [20]. Examples of permittivity estimation using time-domain techniques or radar are given, e.g., in [11], [12], [21], and [22]. Detailed analysis of the electromagnetic properties of concrete can be found in [23].

In order to separate the reflections from the front side of the wall from the reflections of the rebar, the duration (T) of the transmitted pulse should satisfy $T \leq T_{\max} = 2d\sqrt{\varepsilon_{\rm r}}/c$, where d is the distance of the rebar from the front side of the wall and c is the propagation speed of the electromagnetic waves in the air. In the considered case, $d = w/2$ and $T_{\max} = 1.2$ ns. (Alternatively, the expected resolution of the system is $\Delta d = 0.5cT/\sqrt{\varepsilon_{\rm r}}$.)

The reflection coefficient of the TM wave at the air-dielectric interface is

$$R(\theta) = \frac{\cos\theta - \sqrt{\varepsilon_{\rm r} - \sin^2\theta}}{\cos\theta + \sqrt{\varepsilon_{\rm r} - \sin^2\theta}}. \tag{3}$$

in the case of small losses. Without loss of generality, we assume that the angle θ is small; hence $R(\theta) \approx R(0)$. To estimate the permittivity, we coherently add signals received by the sensors in the array. The time delay (τ_{ik}) between the ith and kth sensors, according to Fig. 3, is given by

$$\begin{aligned} s_{ik} &= \sqrt{(x_i - x_{\rm w})^2 + (y_{\rm w} - y_i)^2} \\ &\quad + \sqrt{(x_k - x_{\rm w})^2 + (y_{\rm w} - y_k)^2} \\ \tau_{ik} &= s_{ik}/c_0 \end{aligned} \tag{4}$$

where the coordinates $(x_{\rm w}, y_{\rm w})$ give the position of the reflection point on the wall. The focused waveform reads

$$E_0(t) = \frac{1}{NM^2} \sum_{n=1}^{N} \sum_{i=1}^{M} \sum_{k=1}^{M} E_{ik}(n, t + \tau_{ik}) \sqrt{s_{ik}(n)} \tag{5}$$

where $E_{ik}(n,t)$ is the time-domain waveform of the electric field induced in the kth sensor when the ith sensor is excited, and n is the index of the measurement position. The waveform is shifted in the time domain with respect to τ_{ik} to enable coherent summation (focusing) of the received signals. Multiplication by the factor $\sqrt{s_{ik}(n)}$ ensures that all received signals have the same attenuation, corresponding to the attenuation at distance $s = 1$ m.

We calculate the estimate of the reflection coefficient for small θ as

$$\hat{R}(0) = \left(\int_0^T E_0(t) h(t) dt \right) / \left(\int_0^T h^2(t) dt \right) \tag{6}$$

where $h(t - s/c_0)$ is the induced electric field in the sensor that is separated by distance $s = 1$ m from the transmitting sensor (sensors are in vacuum). We will refer to $h(t)$ as the reference pulse. The estimate of the wall permittivity from (3) is

$$\hat{\varepsilon}_{\rm r} = \left(\frac{1 - \hat{R}(0)}{1 + \hat{R}(0)} \right)^2. \tag{7}$$

B. Wall-Thickness Estimation

The signal reflected from the back side of the wall contains information about the wall thickness. In the case of the reinforced wall, this reflection is concealed by the multiple reflections from the bars. To uncover it, we focus the measured signals in the time domain with respect to the delay of those pulses.

The signal (Fig. 4) transmitted by the ith sensor, reflected from the back side of the wall, and received by the kth sensor is delayed for time

$$\tau_{ik}(w) = \left((2y_w - y_i - y_k)/\cos\theta + 2w\varepsilon_{\rm r}/\sqrt{\varepsilon_{\rm r} - (\sin\theta)^2} \right)/c_0 \tag{8}$$

where

$$\theta = \arg\min_{\theta} \left\{ x_k - x_i - (2y_{\rm w} - y_i - y_k)\tan\theta - 2w\sin\theta/\sqrt{\varepsilon_{\rm r} - (\sin\theta)^2} \right\}. \tag{9}$$

The summation of the received signals, now focused with respect to the delay $\tau_{ik}(w)$, is

$$E_0(t) = \frac{1}{NM^2} \sum_{n=1}^{N} \sum_{i=1}^{M} \sum_{k=1}^{M} E_{ik}\left(n, t + \tau_{ik}(w)\right). \tag{10}$$

The wall thickness is estimated from the correlation of the focused electric field with the reference pulse $h(t)$

$$I(w) = \int_0^T E_0(t) h(t) dt. \tag{11}$$

We calculate the correlation for different wall thicknesses, w. The estimate of the wall thickness is defined as the maximum of (11). Due to the periodic nature of the reflected field, the correlation does not yield a unique solution. Nonetheless, practical limits on the wall thickness reduce the number of estimates to only a few.

IV. Estimation of Target Positions

Movements of people behind the wall perturb the outside antenna measurements. We assume the measurements of the stationary scene behind the wall are available. We obtain the signals reflected from the targets by subtracting the measurements

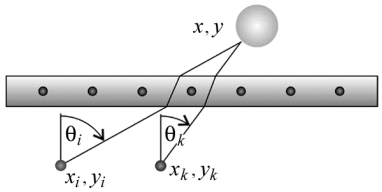

Fig. 5. Position of sensors and target.

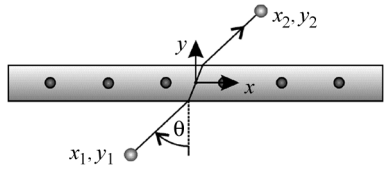

Fig. 6. Position of the sensors for numerical calculation of the wall transmission coefficients.

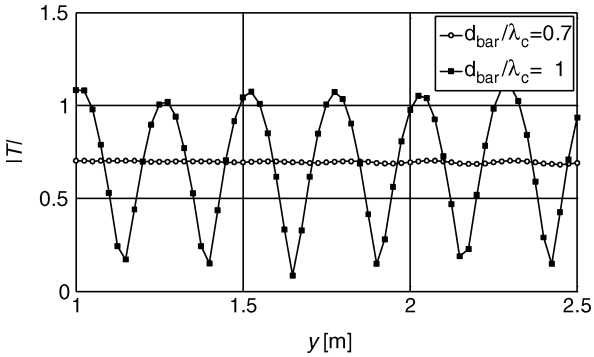

Fig. 7. Transmission coefficient of the wall as a function of the sensor positions. We adopt $x_1 = x_2 = 0$, $y_1 = -y_2 = -y$ (Fig. 6).

of the stationary background from the measurements altered by the appearance of the people. We apply beamforming [1] on the reflected signals to estimate the positions of the moving targets. The proposed technique can be applied in the case for which the characteristics of the bars are unknown. However, we show that the estimation is significantly improved if we have some prior knowledge of the bars.

A. Estimation When Bar Parameters are Unknown

The space behind the wall is divided into small cells [1]. We focus the array response to each cell to determine the presence of the targets. We assume the speed of the electromagnetic waves in the reinforced wall to be the same as the speed in a homogeneous wall of the same permittivity.

If the target is located in the cell with center point (x, y), the kth sensor receives the signal transmitted from the ith sensor delayed for $\tau_i(x,y)+\tau_k(x,y)$, where τ_i, (τ_k) is the signal propagation time from the ith (kth) sensor to the target (Fig. 5)

$$\tau_{i,k}(x,y) = \Big((y - y_{i,k} - w)/\cos\theta_{i,k} + w\varepsilon_{\mathrm{r}}/\sqrt{\varepsilon_{\mathrm{r}} - (\sin\theta_{i,k})^2}\Big)/c_0. \quad (12)$$

The signal transmitted by the ith sensor is launched at angle θ_i, while the kth sensor receives the signal reflected from the target at angle θ_k. Those angles are calculated as

$$\theta_{i,k} = \arg\min_{\theta} \Big\{x - x_{i,k} - (y - y_{i,k} - w)\tan\theta - w\sin\theta/\sqrt{\varepsilon_{\mathrm{r}} - (\sin\theta)^2}\Big\}. \quad (13)$$

We coherently add the received signals with respect to the delay $\tau_i(x,y) + \tau_k(x,y)$. The focused electric field is

$$\Delta E(t;x,y) = \sum_{n=1}^{N}\sum_{i=1}^{M}\sum_{k=1}^{M} \Delta E_{ik}\left(n, t + \tau_i(x,y) + \tau_k(x,y)\right)$$
$$\Delta E_{ik} = E_{ik} - E_{ik}^{\mathrm{stat}} \quad (14)$$

where E_{ik}^{stat} is the induced electric field in the case of the stationary scene and E_{ik} is the induced electric field due to the appearance of the moving objects. The image pixel at (x, y) is obtained by correlating the focused electric field with the reference pulse $h(t)$

$$I(x,y) = \int_0^T \Delta E(t;x,y)h(t)dt. \quad (15)$$

B. Estimation When Bar Parameters are Known

The reference pulse, $h(t)$, represents the waveform of the induced electric field in the receiving sensor for a given excitation waveform. Sensors are assumed to be in a vacuum. The influence of the wall on the received waveform is not taken into account. Here, we model the waveform distortion due to the presence of the wall with bars. We assume that the distance between the bars and their diameter are known. The estimation of the unknown bar parameters is studied in [11], [12]. The authors developed a multiple stratification model of the reinforced concrete, using the characteristic impedance of the wire net derived by Marcuvitz [25].

The transmission coefficient of the reinforced wall for the plane wave incidence is given by

$$T(f,\theta) = E_{\mathrm{t}}/E_{\mathrm{i}} \quad (16)$$

where θ is the incident angle, E_{i} is the incident electric field, and E_{t} is the transmitted electric field. There are several studies of the transmission and reflection coefficients of the infinitely long reinforced wall for the plane-wave incidence, e.g., [8], [9]. For the problem that we consider here, the reinforced wall is not necessarily in the far field of the sensors. Hence, the transmission through the wall depends on the position of the sensors. In order to compute the transmittivity of the wall in the near field, we use the model shown in Fig. 6. We assume that the sensor located at (x_1, y_1) is excited and compute the induced electric field in the sensor located at (x_2, y_2). We define the transmission coefficient as

$$T(f,\theta) = E_{12}(f,\theta)/E_{12}^0(f,\theta) \quad (17)$$

where E_{12} is the induced electric field in the receiving sensor with the wall being present, and E_{12}^0 is the induced electric field when the sensors are in a vacuum. (The dependence of (17) on x_1, y_1, x_2, and y_2 is assumed.)

In Fig. 7, we show the variation of the wall transmission coefficient as a function of the sensor positions for two different values of $d_{\mathrm{bar}}/\lambda_{\mathrm{c}}$ (λ_{c} is the wavelength in the wall). We set the sensor positions to ($x_1 = 0$, $y_1 = -y$) and ($x_2 = 0$, $y_2 = y$).

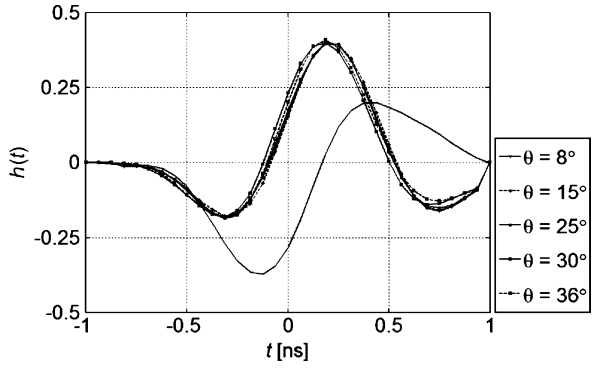

Fig. 8. Normalized pulse shapes $\widetilde{h}(t)$ calculated for various incidence angles. Reference pulse $h(t)$ is denoted by line without markers.

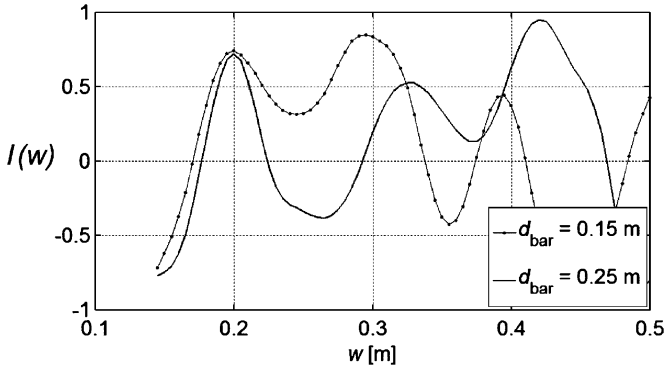

Fig. 9. Estimation of wall thickness: correlation of focused electric field and reference pulse.

In the vicinity of $d_{\rm bar}/\lambda_{\rm c} = 1$, the transmission coefficient of the reinforced wall is periodically dependent on the distance between the sensors and the wall. This result is in agreement with the result reported in [10], where the periodicity of the transmitting characteristics of the reinforced wall was noted.

The distances between the sensors and the wall affect the amplitude of the received signal; their influence on the waveform of the received signal is negligible (up to the scaling constant). Since we are interested in the shape of the received waveform, we compute the transmission coefficients at fixed sensor positions.

The signal reflected from the target behind the wall passes through the wall twice. For the target from Fig. 5, the signal transmitted at angle θ_i passes through the wall, gets reflected from the target, passes again through the wall, and reaches the sensor at angle θ_k. The induced electric field in the receiving sensor is approximately

$$E_{ik}(f) \sim H(f)T(f,\theta_i)T(f,\theta_k) \tag{18}$$

where $H(f)$ is the Fourier transform of $h(t)$. Hence, we adopt for a new reference pulse:

$$\widetilde{h}(t) = \mathrm{rect}\left(\frac{t}{T}\right) F^{-1}\{AH(f)T(f,\theta_i)T(f,\theta_k)\exp(\mathrm{j}2\pi f\tau_0)\} \tag{19}$$

where τ_0 is the time delay that assures that the reference pulse is centered at $t = 0$, and A is the normalization constant.

In Fig. 8 we show the waveforms induced in the receiving sensor after reflecting from PEC behind the wall (inset of Fig. 2). The waveforms are calculated for various angles of incidence, normalized, and centered at $t = 0$. In the same figure, we also show the reference pulse $h(t)$, denoted by the solid line. Since the pulse shape does not vary notably with the incident angle, we use the approximation of (19) for the reference pulse:

$$\widetilde{h}(t) = \mathrm{rect}\left(\frac{t}{T}\right) F^{-1}\left\{AH(f)\left(T(f,0^\circ)\right)^2\exp\left(\mathrm{j}2\pi f\tau_0\right)\right\}. \tag{20}$$

V. Results

We use the electromagnetic solver from Section II to simulate the measurements of the scene behind a reinforced wall. The number of moving objects, as well as their properties, is unknown.

We assume a wall of thickness $w = 0.2$ m and length 8 m. We consider various bar periods: $d_{\rm bar} = 0.15$ m, $d_{\rm bar} = 0.1$ m, and $d_{\rm bar} = 0.05$ m. The bar diameter is set to $D_{\rm bar} = 1$ cm. The adopted relative permittivity of the wall material is $\varepsilon_{\rm r} = 3 - \mathrm{j}0.15$. The moving objects are modeled as perfectly conducting cylinders of radius $r = 0.2$ m, centered at $x = 1$ m, $y = 1.2$ m and $x = -1.5$ m, $y = 0.75$ m, respectively. Besides the targets, there are static (clutter) objects representing furniture and interior walls. We modeled the static objects as dielectric rectangles. The adopted relative permittivity for the static objects is the same as the wall permittivity.

The measuring system consists of a uniform linear array of $M = 3$ sensors. The separation between adjacent sensors is 0.4 m. The array moves parallel to the wall at a distance of 0.75 m from the front side of the wall. The array takes measurements every 0.2 m. The total number of measurement locations is 32.

The sensors transmit a Gaussian pulse, $g(t)$, defined in Section II-C. We also examine the cases in which the spectrum of the signal is shifted in the frequency domain, i.e., $G(f - f_0)$, $0 \le f_0 \le 1$ GHz. The frequency response is calculated from 5 MHz to 2 GHz in 5 MHz steps.

The measurements are corrupted with white noise. We calculate the signal-to-noise ratio with respect to the power of the electric field induced in the sensor. Most of the induced electric field is due to the direct coupling between the sensors. The power of the electric field scattered from the target is several orders of magnitude less than the total electric field induced in the sensor. For this reason, the signal-to-noise ratio cannot be very low.

A. Unknown Bar Parameters

In this example we set $d_{\rm bar} = 15$ cm and $f_0 = 0$. Using (3)–(7), we obtain $\hat{\varepsilon}_{\rm r} = 3$ for the estimate of the wall permittivity. We apply (11) to compute the estimate of the thickness. The result is shown in Fig. 9. The dotted curve represents the correlation of the reference pulse and the focused electric field. There is a maximum corresponding to the real wall thickness, $\hat{w} = 0.2$ m. There are also maxima for $\hat{w} = 0.3$ m and $\hat{w} = 0.4$ m. These other maxima are a consequence of the focusing reflections from the bars. The separation between the maxima depends on the bar period. For comparison, we repeat

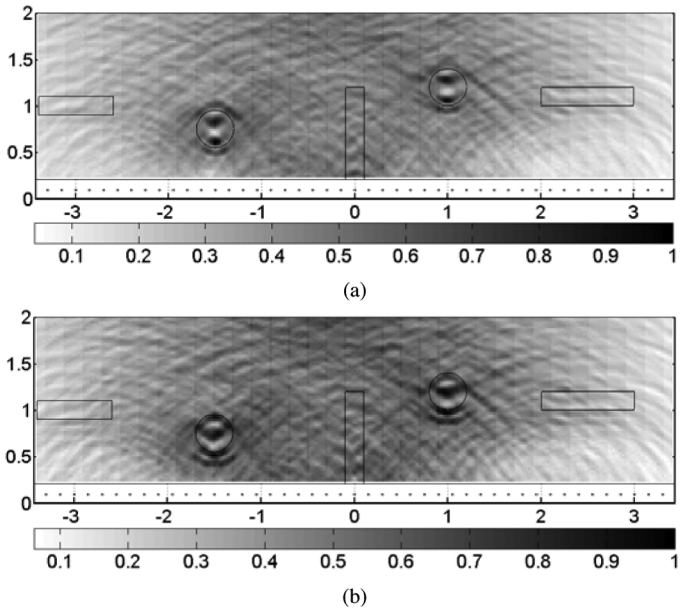

Fig. 10. Image of the scene behind the wall computed using $\varepsilon_{\rm r} = 3$, $f_0 = 0$, and (a) $w = 0.2$ m (real wall thickness) and (b) $w = 0.3$ m (erroneous wall thickness). The waveform distortion is *not* taken into account. The rebar period ($d_{\rm bar} = 15$ cm) is assumed to be unknown. The adopted SNR is 30 dB.

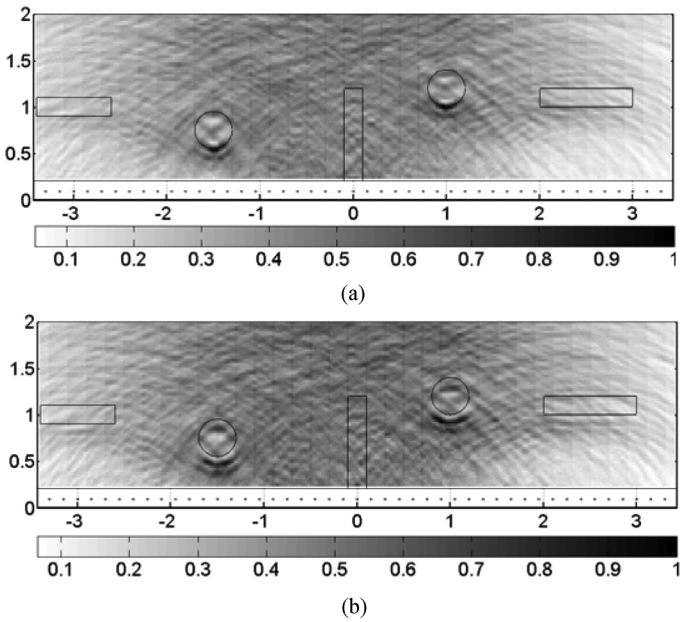

Fig. 11. Image of the scene behind the wall computed using $\varepsilon_{\rm r} = 3$, $f_0 = 0$, and (a) $w = 0.2$ m (real wall thickness) and (b) $w = 0.3$ m (erroneous wall thickness). The waveform distortion is taken into account. The rebar period ($d_{\rm bar} = 15$ cm) is assumed to be known. The adopted SNR is 30 dB.

the analysis for the case in which the bar period is $d_{\rm bar} = 25\,{\rm cm}$ and all other parameters are the same. The result is also shown in Fig. 9 (solid line). Again, we have a maximum corresponding to the real wall thickness, $\hat{w} = 0.2$ m, as well as other spurious maxima. Hence, the beamforming does not produce a unique value for the wall thickness.

We estimate the position of the targets using the wall permittivity and thickness estimates: $\hat{\varepsilon}_{\rm r} = 3$, $\hat{w} = 0.2$ m and $\hat{\varepsilon}_{\rm r} = 3$, $\hat{w} = 0.3$ m, along with $d_{\rm bar} = 15$ cm. The adopted signal-to-noise ratio is $SNR = 30$ dB. (The power of the field reflected from the targets is 20 dB less than the power of the total field induced in the sensors.) The image calculated using the exact wall thickness is shown in Fig. 10(a), and the image calculated using the erroneous wall thickness is shown in Fig. 10(b). The black lines denote the true positions of the cylinders and clutter objects. Due to the oscillating nature of the reflected signal, the images are blurred. The blurriness is more pronounced when the erroneous wall thickness is used [Fig. 10(b)].

B. Modeling Bar Distortion

When the bar characteristics are unknown, the analysis reduces to the case in which the objects are hidden behind a homogeneous wall of the same permittivity. However, the target spreads calculated in this way may be large. If information about the bars is available, we can refine the estimation by modeling the influence of the bars on the signal waveform. We examine this improvement for various bar periods and different frequency content of the excitation waveform.

We repeat the experiment from Fig. 10 assuming the bar parameters are known. The images are calculated using $\hat{\varepsilon}_{\rm r} = 3$, $\hat{w} = 0.2$ m [Fig. 11(a)] and $\hat{\varepsilon}_{\rm r} = 3$, $\hat{w} = 0.3$ m [Fig. 11(b)]. The image quality [Fig. 11(a)] is significantly improved when the corrected pulse shape $\widetilde{h}(t)$ is used compared with the case in which the distortion is not modeled [Fig. 10(a)]. The pixels with the most intensive colors now clearly represent the contours of the objects (as seen by the sensors). The image obtained using erroneous wall thickness is again more blurred [Fig. 11(b)].

We further study the influence of the SNR on the estimation accuracy. We compute the image of the same scene for $SNR = 10$ dB, which is anticipated as the signal-to-noise threshold in this example. The target traces are clearly visible if the bar parameters are known [Fig. 12(a)]. In contrast, for low SNR, the targets cannot be discerned without waveform correction [Fig. 12(b)].

Transmission and reflection coefficients of the reinforced wall are greatly influenced by the ratio of the signal wavelength and the bar spacing, [8], [9], [11], [12]. The investigations in [11], [12] showed that when the ratio $d_{\rm bar}/\lambda_{\rm c}$ is decreased to 0.3–0.4, the transmittivity of the wall is significantly reduced due to the rebar. Conversely, the influence of the bars is reduced if $d_{\rm bar}/\lambda_{\rm c}$ is larger than 0.7–0.8. We study those results in the context of the through-the-wall imaging.

As the central frequency of the pulse spectrum increases, the position of the targets can be estimated even in the case for which the bar parameters are unknown. Our simulations showed that in the considered example ($d_{\rm bar} = 15\,{\rm cm}$, $SNR = 10\,{\rm dB}$), without prior knowledge of the bar parameters, the minimal central frequency that allows estimating targets is $f_0 = 0.5$ GHz. This finding is in agreement with the results from [11], [12], that showed that the attenuation is significant for all frequencies smaller than 0.5 GHz for given wall parameters. In Fig. 13 we show the results obtained without the correction, for $f_0 = 0.5$ GHz and $f_0 = 1$ GHz.

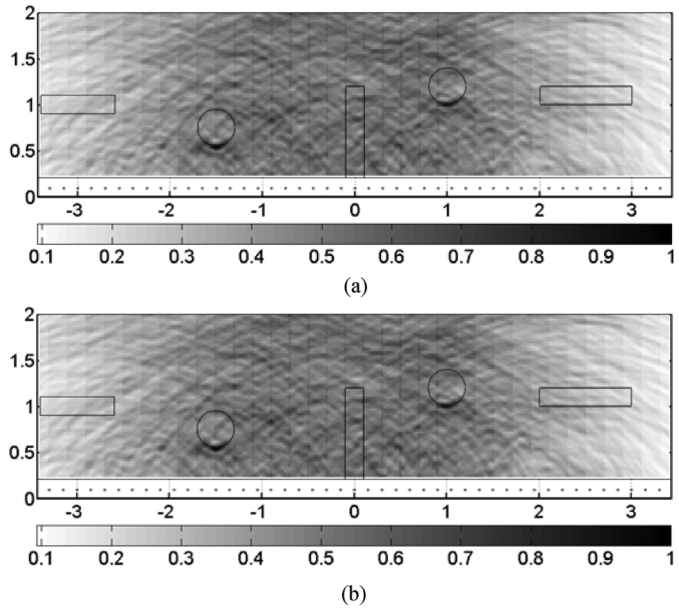

Fig. 12. Image of the scene behind the wall computed for $SNR = 10$ dB, $\varepsilon_r = 3$, $w = 0.2$ m, $d_{\rm bar} = 15$ cm, and $f_0 = 0$. The waveform distortion is (a) taken and (b) *not* taken into account.

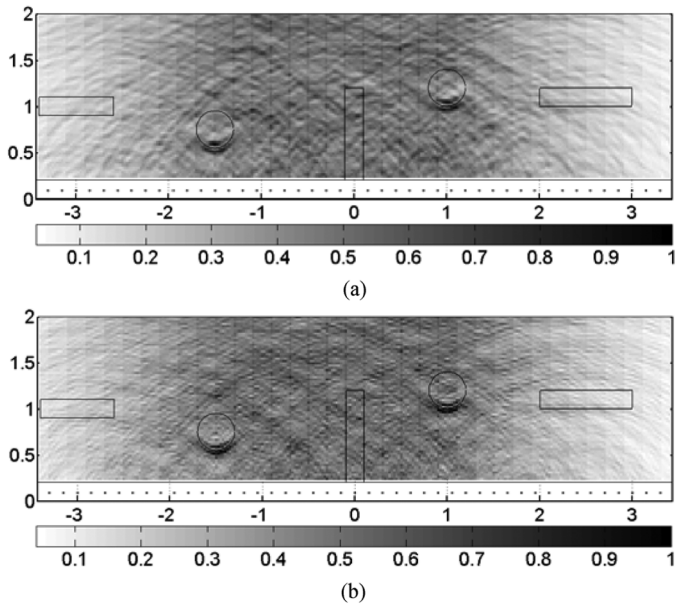

Fig. 13. Image of the scene behind the wall computed for $SNR = 10$ dB, $\varepsilon_r = 3$, $w = 0.2$ m, $d_{\rm bar} = 15$ cm, and (a) $f_0 = 0.5$ GHz and (b) and $f_0 = 1$ GHz. The waveform distortion is *not* taken into account.

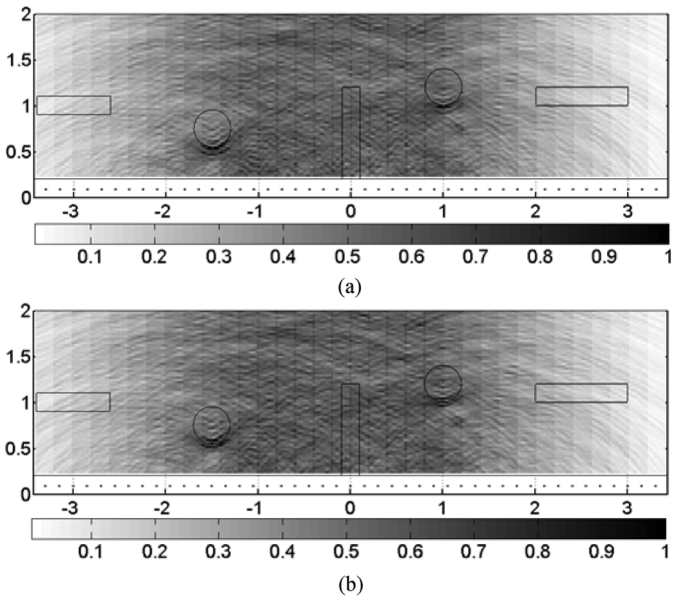

Fig. 14. Image of the scene behind the wall computed for $SNR = 15$ dB, $\varepsilon_r = 3$, $w = 0.2$ m, $d_{\rm bar} = 10$ cm, and $f_0 = 0.75$ GHz. The waveform distortion is (a) taken and (b) *not* taken into account.

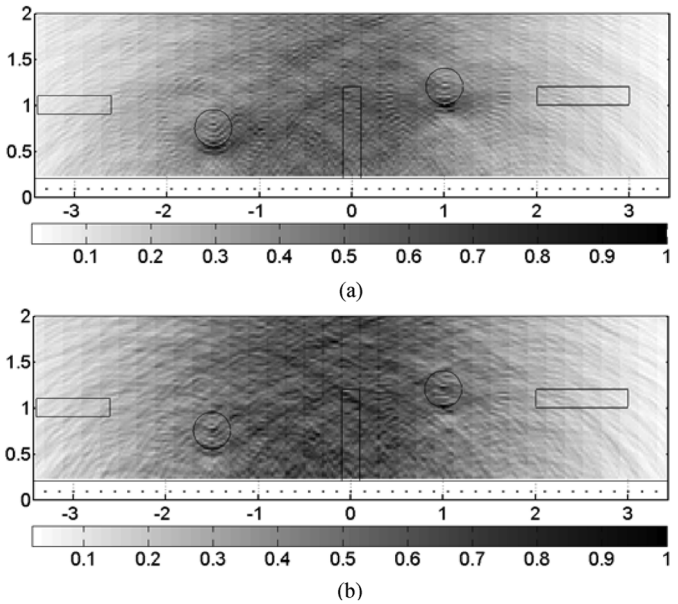

Fig. 15. Image of the scene behind the wall computed for $SNR = 20$ dB, $\varepsilon_r = 3$, $w = 0.2$ m, $d_{\rm bar} = 6$ cm, and $f_0 = 1$ GHz. The waveform distortion is (a) taken and (b) *not* taken into account.

We repeated the experiment for $d_{\rm bar} = 10$ cm and $SNR = 15$ dB (Fig. 14). The improvement due to the waveform correction is significant for $f_0 \leq 0.75$ GHz, while there is almost no difference at $f_0 = 1$ GHz. According to [11], [12], in this case, the rebar has major influence for frequencies smaller than 0.7 GHz.

Finally, for $d_{\rm bar} = 6$ cm, it was expected that the improvement would be significant for $f_0 \leq 1$ GHz. (For $d_{\rm bar} = 6$ cm the attenuation is considerable for frequencies smaller than 1 GHz.) Our computations confirm this conclusion. In Fig. 15 we show the images computed for $f_0 = 1$ GHz and $SNR = 20$ dB, with and without correction.

We examined the robustness of the algorithm to the errors in bar parameters. In Fig. 16 we show the results obtained assuming that the bar period was $d_{\rm bar} = 10$ cm, while the true value was $d_{\rm bar} = 15$ cm. The image does not differ significantly from the image obtained with real wall parameters [Fig. 12(a)].

VI. Conclusion

We addressed the important problem in urban warfare of estimating moving targets, such as personnel, behind a reinforced

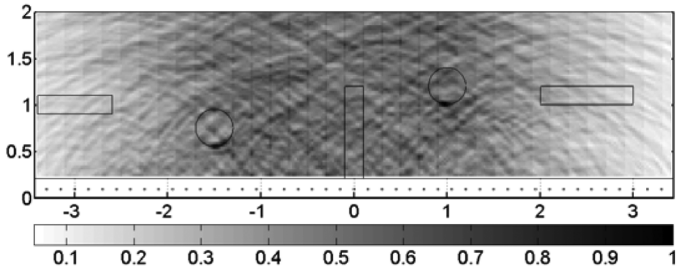

Fig. 16. Image of the scene behind the wall computed for $SNR = 10$ dB, $\varepsilon_r = 3$, $w = 0.2$ m, $d_{\text{bar}} = 15$ cm, and $f_0 = 0$ GHz. Waveform distortion is modeled using erroneous bar period ($d_{\text{bar}} = 10$ cm).

wall, using radar measurements. Reinforced walls significantly attenuate low frequencies and distort the transmitted waveforms. The signals reflected from the objects behind reinforced walls are oscillating in nature and are of long duration because of the bar periodic arrangement. First, we considered the case in which the reinforced wall is completely unknown. We added coherently measured electric fields in various time gates to estimate wall thickness and concrete permittivity independently. We assumed the availability of the measurements of the static scene behind the wall (walls, furniture, etc.) and measurements altered by the appearance of people. The difference between these two measurements is associated with the electromagnetic field scattered from the moving targets. We applied beamforming to the field reflected from the targets to estimate their number and locations. The algorithm performed satisfactorily in the case in which the bar diameter and period are both unknown. However, due to multiple echoes, the target spreads are large. We also analyzed the problem in which the characteristics of the metallic rebar are known. We improved the estimation significantly by modeling the waveform distortion due to the bars. The resulting images are focused and accurately represent the contours of the targets. The algorithm is robust to the ambiguities in bar parameter values. In addition, the minimal necessary SNR is lower compared with the case in which the influence of the bars on the signal shape is ignored.

REFERENCES

[1] F. Ahmad, M. G. Amin, and S. A. Kassam, "Synthetic aperture beamformer for imaging through a dielectric wall," *IEEE Trans. Aerosp. Electron. Syst.*, vol. 41, no. 1, pp. 271–283, Jan. 2005.

[2] F. Ahmad and M. G. Amin, "A noncoherent radar system approach for through-the-wall imaging," in *Proc. SPIE*, Bellingham, WA, Mar. –April 2005, vol. 5778, Sensor, and Command, Control, Communications, and Intelligence Technologies for Homeland Security and Homeland Defense IV.

[3] G. Wang and M. Amin, "Imaging through unknown walls using different standoff distances," *IEEE Trans. Signal Processing*, vol. 54, no. 10, pp. 4015–4025, Oct. 2006.

[4] A. R. Hunt, "Image formation through walls using a distributed radar sensor network," presented at the IEEE AP-S Int. Symp. USNC/URSI Nat. Radio Science Meeting, Monterey, CA, Jun. 2004.

[5] D. G. Falconer, K. N. Steadman, and D. G. Watters, "Through-the wall differential radar," in *Proc. SPIE*, Boston, MA, Nov. 1996, vol. 2938, Enabling Technologies for Law Enforcement, pp. 147–151.

[6] M. Dehmollaian and K. Sarabandi, "Simulation of through-wall microwave imaging: Forward and inverse models," presented at the Proc. of IEEE Int. Geosci. and Remote Sensing Symp., 2006.

[7] M. Nikolic, M. Ortner, A. Nehorai, and A. Djordjevic, "Estimating building layouts using radar and jump-diffusion algorithm," *IEEE Trans. Antennas Propag.*, vol. 57, no. 3, pp. 768–776, Mar. 2009.

[8] E. Richarlot, M. Bonilla, W. Wong, V. Fouad-Hanna, H. Baudrand, and J. Wiart, "Electromagnetic propagation into reinforced concrete walls," *IEEE Trans. Microw. Theory Tech.*, vol. 48, pp. 357–366, Mar. 2000.

[9] R. A. Dalke, C. L. Holloway, P. McKenna, M. Johansson, and A. S. Ali, "Effects of reinforced concrete structures on RF communications," *IEEE Trans. Electromagn. Compat.*, vol. 42, pp. 486–496, Nov. 2000.

[10] R. Paknys, "Reflection and transmission by reinforced concrete-numerical and asymptotic analysis," *IEEE Trans. Antennas Propag.*, vol. 51, no. 10, pp. 2852–2861, Oct. 2003.

[11] H. Chiba and Y. Miyazaki, "Reflection and transmission characteristics of radio waves at a building site due to reinforced concrete slabs," *Electron. Commun. Jpn. (Part I: Commun.)*, vol. 81, no. 8, pp. 68–80, 1998.

[12] H. Chiba and Y. Miyazaki, "Dependence of radio wave reflection and transmission characteristics of reinforced concrete slabs on frequency and angle of incidence," *Electron. Commun. Jpn. (Part I: Commun.)*, vol. 85, no. 1, pp. 69–81, 2002.

[13] H. L. R. Chen, U. B. Halabe, Z. Sami, and V. Bhandarkar, "Impulse radar reflection waveforms of simulated concrete bridge decks," *Mater. Eval.*, vol. 52, no. 12, pp. 1382–1388, 1994.

[14] U. B. Halabe, K. R. Maser, and E. A. Kausel, "Condition assessment of reinforced concrete structures using electromagnetic waves," *ACI Mater. J.*, vol. 92, no. 5, pp. 511–523, Sep. 1995.

[15] G. Antonini, A. Orlandi, and S. D'elia, "Shielding effects of reinforced concrete structures to electromagnetic fields due to GSM and UMTS systems," *IEEE Trans. Magn.*, vol. 39, no. 3, pp. 1582–1585, May 2003.

[16] S. V. Savov and M. H. A. J. Herben, "Modal transmission-line modeling of propagation of plane radiowaves through multilayer periodic building structures," *IEEE Trans. Antennas Propag.*, vol. 51, pp. 2244–2251, Sep. 2003.

[17] R. F. Harrington, *Field Computation by Moment Methods*. Malabar, FL: Krieger, 1982.

[18] A. R. Djordjević, T. K. Sarkar, and S. M. Rao, "Analysis of finite conductivity cylindrical conductors excited by axially-independent TM electromagnetic field," *IEEE Trans. Microw. Theory Techn.*, vol. MTT-33, no. 10, pp. 960–966, Oct. 1985.

[19] D. M. Pozar, *Microwave Engineering*, 3rd ed. New York: Wiley, 2005.

[20] T. Chung, C. R. Carter, T. Masliwec, and D. G. Manning, "Impulse radar evaluation of concrete, asphalt and waterproofing membrane," *IEEE Trans. Aerosp. Electron. Syst.*, vol. 30, no. 2, pp. 404–415, Apr. 1994.

[21] R. H. Cole, J. G. Berberian, S. Mashimo, G. Chryssikos, A. Burns, and E. Tombary, "Time domain reflection methods for dielectric measurements to 10 GHz," *J. Appl. Phys.*, vol. 66, no. 2, Jul. 1989.

[22] N. E. Hager, III and R. C. Domszy, "Monitoring of cement hydration by broadband time-domain-reflectometry dielectric spectroscopy," *J. Appl. Phys.*, vol. 96, no. 9, Nov. 2004.

[23] U. B. Halabe, A. Sotoodehnia, K. R. Maser, and E. A. Kausel, "Modeling the electromagnetic properties of concrete," *ACI Mater. J.*, vol. 90, no. 6, pp. 552–563, Nov. 1993.

[24] P. D. Walker and M. R. Bell, "Subsurface permittivity estimation from ground-penetrating radar measurements," presented at the IEEE Int. Radar Conf., 2000.

[25] N. Marcuvitz, *Waveguide Handbook*. New York: McGraw-Hill, 1951.

Marija M. Nikolic received the B.Sc., M.Sc., and Ph.D. degrees from the University of Belgrade, Belgrade, Serbia, in 2000, 2003, and 2007, respectively.

In 2001, she joined the School of Electrical Engineering, University of Belgrade, as a Teaching Assistant where, in 2008, she was promoted to an Assistant Professor. Currently, she is working toward the Ph.D. degree at Washington University in St. Louis. She is interested in numerical electromagnetics applied to signal processing, antennas analyses and design, and MIMO systems.

Arye Nehorai (S'80–M'83–SM'90–F'94) received the B.Sc. and M.Sc. degrees in electrical engineering from the Technion—Israel Institute of Technology, Haifa, and the Ph.D. degree in electrical engineering from Stanford University, Stanford, CA.

From 1985 to 1995, he was a faculty member with the Department of Electrical Engineering, Yale University. In 1995, he joined the Department of Electrical Engineering and Computer Science, The University of Illinois at Chicago (UIC), as Full Professor where, from 2000 to 2001, he was Chair of the department's Electrical and Computer Engineering (ECE) Division, which then became a new department. In 2001, he was named University Scholar of the University of Illinois. In 2006, he became Chairman of the Department of Electrical and Systems Engineering, Washington University in St. Louis. He is the inaugural holder of the Eugene and Martha Lohman Professorship and the Director of the Center for Sensor Signal and Information Processing (CSSIP) at WUSTL since 2006.

Dr. Nehorai has been a Fellow of the IEEE since 1994 and of the Royal Statistical Society since 1996. He was co-recipient of the IEEE SPS 1989 Senior Award for Best Paper, coauthor of the 2003 Young Author Best Paper Award, and co-recipient of the 2004 Magazine Paper Award. He was elected Distinguished Lecturer of the IEEE SPS for the term 2004 to 2005 and received the 2006 IEEE SPS Technical Achievement Award. He is the Principal Investigator of the new multidisciplinary university research initiative (MURI) project entitled Adaptive Waveform Diversity for Full Spectral Dominance. He was Editor-in-Chief of the IEEE TRANSACTIONS ON SIGNAL PROCESSING during the years 2000 to 2002. From 2003 to 2005, he was Vice President (Publications) of the IEEE Signal Processing Society, Chair of the Publications Board, member of the Board of Governors, and member of the Executive Committee of this Society. From 2003 to 2006, he was the Founding Editor of the special columns on Leadership Reflections in *IEEE Signal Processing Magazine*.

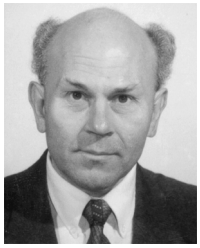

Antonije R. Djordjević was born in Belgrade, Serbia, on April 28, 1952. He received the B.Sc., M.Sc., and D.Sc. degrees from the School of Electrical Engineering, University of Belgrade, in 1975, 1977, and 1979, respectively.

In 1975, he joined the School of Electrical Engineering, University of Belgrade, as a Teaching Assistant. He was promoted to an Assistant Professor, Associate Professor, and Professor, in 1982, 1988, and 1993, respectively. In 1983, he was a Visiting Associate Professor at Rochester Institute of Technology, Rochester, NY. Since 1992, he has been an Adjunct Scholar with Syracuse University, Syracuse, NY. In 1997, he became a Corresponding Member of the Serbian Academy of Sciences and Arts, and he became a full member in 2006. His main area of interest is numerical electromagnetics, in particular applied to fast digital signal interconnects, wire and surface antennas, microwave passive circuits, and electromagnetic-compatibility problems.